The Scientific Temper
AUGUST 2026 Vol. 17 (8): 6757-6779
ISSN: 0976-8653, E-ISSN: 2231-6396
DOI: 10.58414/SCIENTIFICTEMPER.2026.17.8.2529
A WEB OF SCIENCE JOURNAL

RESEARCH ARTICLE

Multilevel Thresholding Medical Image Segmentation Using Adaptive Entropy-Regulated Particle Swarm Optimization

J. HAJIRAM BEEVI[1], O.A. MOHAMED JAFAR[2], A.R. MOHAMED SHANAVAS[3]

[1]*Research Scholar, PG and Research Department of Computer Science, Jamal Mohamed College (Autonomous), Affiliated to Bharathidasan University, Tiruchirappalli – 620020, India. Email id: haji123k@gmail.com*

[2]*Associate Professor, PG and Research Department of Computer Science, Jamal Mohamed College (Autonomous), Affiliated to Bharathidasan University, Tiruchirappalli – 620020, India. Email id: mohamedjafaroa@gmail.com*

[3]*Associate Professor, PG and Research Department of Computer Science, Jamal Mohamed College (Autonomous), Affiliated to Bharathidasan University, Tiruchirappalli – 620020, India. Email id: arms3375@gmail.com*

Corresponding Author*: haji123k@gmail.com

ABSTRACT

Image segmentation clusters pixels with common intensity characteristics into different regions. Multilevel thresholding is one of the most commonly used segmentation techniques because it requires relatively low computational effort while producing satisfactory results for many applications. The main challenge is selecting threshold values that maximize segmentation quality. Standard Particle Swarm Optimization (PSO) may get trapped in local optima before finding better threshold combinations, especially when dealing with complicated search spaces. To overcome this limitation, an Adaptive Entropy-Regulated Particle Swarm Optimization (AER-PSO) algorithm is developed for multilevel threshold selection. In the proposed algorithm, a particle encodes a set of threshold values, and Kapur's entropy defines the optimization objective. Normalized swarm entropy is used to estimate swarm diversity and adaptively regulate the inertia weight, while Gaussian perturbation is applied to particle velocities during low-diversity states to enhance exploration and prevent premature convergence. The proposed method is evaluated against PSO, Quantum Particle Swarm Optimization (QPSO), and Pyramid Particle Swarm Optimization with Complementary Inertia Weights (CIWP-PSO). The evaluation is performed using the same high-bit-depth medical image dataset employed in the original CIWP-PSO study, as well as the publicly available BrainWeb and Internet Brain Segmentation Repository (IBSR) datasets. Experimental results show that AER-PSO consistently achieves higher Kapur entropy and outperforms the compared algorithms in terms of Segmentation Accuracy, Jaccard Similarity, Dice Similarity, Sensitivity, Peak Signal-to-Noise Ratio (PSNR), Structural Similarity Index Measure (SSIM), and Feature Similarity Index Measure (FSIM). The novelty of AER-PSO lies in its entropy-regulated adaptive inertia weight mechanism integrated with Gaussian velocity perturbation, which dynamically balances exploration and exploitation, maintains swarm diversity, prevents

Received: 15th August, 2026 **Accepted: 17th August, 2026** **Published: 28th August, 2026**

premature convergence, and achieves superior multilevel threshold optimization and image segmentation performance compared with existing PSO-based methods.

Keywords: *Image Segmentation, Multilevel Thresholding, Particle Swarm Optimization, Adaptive Inertia Weight, Swarm Entropy.*

INTRODUCTION

Image segmentation is an important method of image processing and computer vision in which the segmentation of an image takes place by separating pixels of the image into different regions called segments based on their similarity. These segments are generally corresponding to objects, foreground, or background parts of an image. As opposed to image recognition, in which the main concern is the identification of objects of the image, image segmentation involves dividing the image into various regions so that the task of analyzing the image becomes easier. Segmentation involves partitioning the image into several regions that can be analyzed easily and efficiently for better computer processing of images (Pal & Pal, 1993).

The process of image segmentation is important in making image processing tasks more efficient and accurate. It is useful as the preliminary process in the analysis of images since it assists in detecting objects, extracting features, classifying and recognizing images. Due to its capability of identifying regions of interest in images, image segmentation has been widely applied in numerous domains including medical imaging where it is used for the identification of tumors or lesions, bio metric systems for fingerprint recognition, remote sensing for land cover classification, and computer vision for automatic object analysis. Consequently, image segmentation has become an essential component of modern image analysis systems across scientific, industrial, and healthcare applications.

Among these applications, medical image segmentation is particularly important because accurate delineation of anatomical structures and pathological regions directly influences disease diagnosis, treatment planning, surgical navigation, and quantitative assessment of anatomical structures. However, medical image segmentation is substantially more challenging than normal image segmentation owing to various issues such as noise, low contrast, intensity inhomogeneity, blurry object borders, and variations in patient anatomy. Moreover, different medical imaging techniques such as MRI, CT, and X-ray images have their distinct characteristics, making it more difficult for segmenting images. Changes in quality of the image, contrast, intensity, and anatomy make

it necessary for an algorithm to have robust optimization abilities in order to be able to detect regions of interest and make it more effective for computer aided diagnosis of the image (Pham et al., 2000).

Among various segmentation techniques, threshold-based segmentation has attracted considerable attention because of its simplicity, computational efficiency, and effectiveness in separating image regions according to pixel intensity. In particular, multilevel thresholding has been widely employed in medical image analysis because it enables the extraction of multiple anatomical structures and pathological regions simultaneously. However, finding the optimal threshold values is difficult when the number of thresholds increases, which makes image segmentation a complex optimization problem (Sahoo et al., 1988).

Entropy-based thresholding methods have been widely adopted because they maximize the information content between segmented regions, allowing more effective separation of complex image structures while preserving important image information (Kapur et al., 1985). Consequently, entropy-based multilevel thresholding has become one of the most widely adopted optimization criteria for medical image segmentation, particularly in MRI and CT image analysis where accurate threshold selection is critical. However, identifying the optimal threshold values using entropy-based criteria remains a computationally challenging optimization problem, particularly for multilevel segmentation.

However, owing to the limitations of traditional approaches for threshold optimization, many research studies have used the concept of metaheuristic optimization techniques like Genetic Algorithm, Differential Evolution, Ant Colony Optimization and Particle Swarm Optimization. Among these techniques, PSO has become one of the most popular population-based optimization algorithms because of its simple implementation, fewer control parameters, low computational complexity, and rapid convergence. PSO is a computational method that simulates the social behavior of flocks of birds and schools of fish by updating position and velocity of particles through individual and collective experience. These characteristics make PSO particularly suitable for multilevel threshold optimization in image segmentation (Maitra & Chatterjee, 2007).

Some of the more recently proposed improved PSO algorithms are chaotic PSO, adaptive PSO, opposition-based PSO, elite particle PSO, and hybrid PSO algorithms. These improved algorithms aim at improving convergence speed, diversity of search, and accuracy of segmentation. Despite these advancements, existing PSO-based segmentation methods still suffer from premature convergence, loss of swarm diversity, and entrapment in local optima, particularly when solving high-dimensional multilevel threshold optimization problems (Liang et al., 2006). Moreover, most existing methods rely on predefined parameter adjustment strategies and do not explicitly regulate the optimization process according to the current diversity of the particle swarm. While entropy has been extensively employed as an objective function for threshold selection, it has rarely been utilized as a feedback mechanism to guide the optimization behavior itself. Thus, the aim of this research is to devise an adaptive PSO algorithm which regulates its behavior based on the diversity within the swarm, and as a consequence enhances the segmentation of medical images.

To the best of our knowledge, existing entropy-based PSO approaches primarily employ entropy to evaluate threshold quality rather than to regulate swarm behavior during optimization. In contrast, the proposed method utilizes swarm entropy as an adaptive feedback mechanism to continuously monitor particle diversity throughout the optimization process. Swarm entropy provides a quantitative measure of particle diversity, reflecting the current search state of the particle population. It enables the algorithm to adaptively regulate exploration and exploitation according to the optimization progress, thereby reducing premature convergence while maintaining efficient convergence toward the global optimum.

Consequently, this research work proposes an Adaptive Entropy-Regulated Particle Swarm Optimization (AER-PSO) algorithm for medical image segmentation. The proposed framework integrates swarm entropy analysis, adaptive inertia weight regulation, and random perturbation within a unified PSO architecture. As per the calculated swarm entropy value, the inertia weight is dynamically adjusted to balance global exploration and local exploitation. Whenever the diversity of the swarm falls below a certain threshold level, then random perturbation is applied to enhance the population diversity and prevent premature convergence. Through this adaptive regulation mechanism, the proposed AER-PSO achieves more effective threshold optimization and improved segmentation performance for complex medical images.

The main contributions of the proposed AER-PSO algorithm are summarized as follows:

- An entropy-regulated swarm diversity mechanism that continuously monitors particle distribution during the optimization process.
- An adaptive inertia weight strategy that dynamically balances global exploration and local exploitation according to swarm entropy.
- A random perturbation technique that increases swarm diversity and avoids early convergence while performing threshold optimization.
- A unified adaptive PSO framework that improves convergence stability and segmentation accuracy for medical image analysis.

The effectiveness of the proposed AER-PSO algorithm is evaluated on BRAINWEB and IBSR medical image datasets using standard segmentation quality metrics and compared with several state-of-the-art PSO-based optimization algorithms to demonstrate its convergence efficiency and segmentation performance.

The remainder of this paper is organized as follows. Section 2 reviews the related works, including the theoretical background of PSO and existing PSO-based image segmentation methods. Section 3 explains the proposed AER-PSO algorithm. Section 4 gives the experimental setup, datasets, evaluation metrics, and results with discussion. Section 5 presents the conclusion and outlines the future scope of the work.

LITERATURE REVIEW

This section presents the background of PSO and reviews related studies that have used PSO and its variants for image segmentation.

Particle Swarm Optimization (PSO)

Kennedy and Eberhart presented PSO in the year 1995. The method is based on the way bird flocks move and share information while searching for better positions. In PSO, each possible solution is considered as a particle, and a set of particles forms a swarm. The particles move in the search space to obtain an optimal solution.

The position update of each particle is based on its velocity, personal best position (P_{best}), and global best position (G_{best}) of the swarm. The inertia weight affects the movement of particles by controlling the balance between exploration and exploitation. Large inertia weights lead to a broadened search space for the particles while small values assist the particles in refining their current solutions. Although PSO is simple and effective, it can suffer from premature convergence and loss of swarm diversity when applied to complex problems such as multilevel image thresholding. Therefore, several PSO variants have been developed to improve the search performance (Kennedy & Eberhart, 2002).

Algorithm 1: Standard Particle Swarm Optimization (PSO)

Input: Swarm size N, maximum iterations T_{max}, inertia weight w, acceleration coefficients c_1, c_2

Output: Global best solution G_{best}

1. Initialize swarm size N and maximum number of iterations T_{max}.

2. Initialize inertia weight w, cognitive coefficient c_1, and social coefficient c_2.

3. Randomly initialize particle positions X_i and velocities V_i, where i=1,2,...,N.

4. Evaluate fitness $f(X_i)$for each particle.

5. Set personal best positions:

$$Pbest_i = X_i$$

6. Determine global best position:

$$G_{best} = arg\ min(f(Pbest_i))$$

7. while t < T_{max} do

8. for each particle i=1 to N do

9. Generate random numbers r1, r2 ∈[0,1]

10. Update velocity:

$$V_i(t+1) = wV_i(t) + c_1 r_1 (Pbest_i - X_i(t)) + c_2 r_2 (Gbest_i - X_i(t))$$

11. Update position:

$$X_i(t+1) = X_i(t) + V_i(t+1)$$

12. Evaluate fitness $f(X_i(t+1))$

13. If $f(X_i(t+1))$ is better than $f(Pbest_i)$ then

14. $Pbest_i = X_i(t+1)$

15. End If

16. End for

17. Update global best:

$$G_{best} = arg\ min(f(Pbest_i))$$

18. Update iteration counter t = t + 1

19. End while

20. Return Gbest

PSO-Based Image Segmentation Methods

Image segmentation is an important step in image processing, as it helps to divide an image into meaningful regions for further analysis. Many researchers have used Particle Swarm Optimization (PSO) and its variants for image segmentation because of their ability to search for suitable segmentation thresholds. Several PSO-based image segmentation methods have been proposed in previous studies. Some of the methods reported by different researchers are reviewed as follows:

Mahalakshmi and Velmurugan (2015) proposed an image segmentation technique for detection of brain tumors using PSO. The steps involved in the algorithm include DICOM image conversion, image segmentation using PSO, selection of best segmented images, and selection of tumor region. Experimental results reveal that PSO is useful in detecting the tumor affected area with higher accuracy through segmentation level adjustment.

Dhieb and Frikha (2016) introduced a PSO-based multilevel thresholding approach for segmenting images. The technique finds the best threshold value by maximization of both Kapur's entropy and Otsu's function. Experiments carried out on grayscale and MRI images proved that the new approach offered better segmentation performance while consuming lesser computation time than conventional methods.

Lokhande and Pujeri (2018) proposed a PSO-based image segmentation approach for improving clustering and classification of image data. The proposed method uses PSO to find out the best cluster centers by minimizing the objective function based on image features and color histograms. The results shown that the proposed approach effectively performs image segmentation and clustering, showing the capability of PSO in solving complex optimization problems in image analysis.

Dixit and Nanda (2019) used Particle Swarm Optimization (PSO) for brain tumor segmentation in MRI images. Dixit and Nanda applied Particle Swarm Optimization (PSO) to segment brain tumors from MRI images. It used Discrete Wavelet Transform (DWT) to obtain image features and Support Vector Machine (SVM) for classification. In their work, 13 features were used to classify the MRI images as tumorous or non-tumorous. PSO provided accurate tumor regions, and the resulting features gave good classification results with SVM.

Li et al. (2019) developed a Level Set-based medical image segmentation method enhanced with Cooperative Particle Swarm Optimization (CPSO). This method combines CPSO with the Local Binary Fitting (LBF) model in order to avoid problems such as susceptibility to local minimum and contour initialization. The experimental results indicated that the effectiveness and convergence rate have been greatly enhanced by this technique.

Tan et al. (2019) have suggested the use of Enhanced PSO for an ensemble of deep learning algorithms for image segmentation. The approach includes optimizing the hyper-parameters of convolutional neural networks and enhancing the Fuzzy C-Means clustering using the PSO algorithm combined with simulated annealing and differential evolution. Experiments conducted using the dataset of skin lesions and medical images showed better performance in comparison to other deep learning and clustering methods.

Chakraborty et al. (2020) proposed an Improved Particle Swarm Optimization (IPSO)-based Minimum Cross-Entropy Thresholding (MCET) method for multilevel image segmentation. The IPSO method reduces premature convergence by dividing the high-dimensional swarm into one-dimensional swarms. This improves the search for suitable threshold values. Experimental results shown superior segmentation performance, faster convergence, lower computational cost, and better fitness values compared to PSO, Genetic Algorithm, Firefly, Cuckoo Search, and Artificial Bee Colony algorithms.

Lan et al. (2022) suggested an approach called Group Theoretic Particle Swarm Optimization (GT-PSO), which is used for multilevel thresholding lung cancer image segmentation with the use of Kapur's entropy. Applying principles of group theory to the PSO algorithm allowed obtaining a highly accurate segmentation results with high values of precision, recall, F1-Score, and IoU metrics.

Zheng et al. (2022) developed an optimized PSO for OTSU-based multi-threshold image segmentation. The optimization process involves using asynchronous learning factor, chaos optimization, and elite particle search strategies, which increase the speed of search while mitigating early convergence issues. Their experiment using PASCAL 2012 data set found out that the proposed algorithm performed better in terms of segmentation accuracy and convergence speed compared to conventional PSO and other meta-heuristic algorithms.

Ma and Hu (2024) proposed CIWP-PSO (Pyramid Particle Swarm Optimization with Complementary Inertia Weights) to perform multi-threshold image segmentation based on the Kapur entropy objective function. The method adopts a pyramid swarm structure as well as a random opposition learning mechanism to boost its global searching ability and prevent early convergence. It was shown that CIWP-PSO performed better than the existing PSO-based optimization methods in terms of segmentation accuracy and fitness value, especially for medical image segmentation.

Nie et al. (2024) have suggested a multilevel thresholding technique for crack image segmentation using the concept of minimum arithmetic-geometric divergence and an advanced PSO technique. This technique uses the idea of local stochastic perturbation. Comparative performance analysis performed using the DeepCrack dataset showed that the proposed technique outperforms many modern thresholding techniques in terms of both segmentation accuracy and computational efficiency.

Saifullah and Dreżewski (2024) introduced PSO-based Histogram Equalization (PSO-HE) algorithm for medical image segmentation. This algorithm is based on the use of Histogram Equalization for enhancement and PSO for segmentation purposes. Results on segmentation of lung CT scans and chest X-rays using PSO-HE were better than Otsu, Watershed, and K-means, though the algorithm needs more accurate parameter setting and is computationally complex.

Sekar and Parthasarathy (2025) proposed an automatic thresholding method for retinal image segmentation based on particle swarm optimization for the classification of diabetic retinopathy. The optimal thresholds were selected based on entropy as the criterion function and the method was tested on the IDRiD fundus images dataset. It has been proved that the algorithm gives better results than conventional thresholding methods like Otsu and entropy-based methods.

PROPOSED ALGORITHM

This section presents the proposed AER-PSO algorithm for multilevel threshold-based medical image segmentation. Conventional PSO may lose swarm diversity as the search progresses, which can result in premature convergence and an ineffective balance between global exploration and local exploitation. To reduce these effects, the proposed AER-PSO monitors the normalized swarm entropy at each iteration and adjusts the inertia weight according to the current diversity of the swarm. When the swarm enters a low-diversity state, a Gaussian velocity perturbation is applied to encourage exploration and improve the ability of the particles to escape local optima.

In the proposed algorithm, each particle represents a candidate set of multilevel thresholds. Kapur's entropy is used as the objective function to evaluate the quality of each threshold set. During the optimization process, the particles are updated at each iteration to maximize the entropy value. After the optimization is completed, the optimal threshold set is used to produce the segmented medical image.

The proposed AER-PSO framework consists of six stages: (1) particle initialization, (2) swarm entropy computation, (3) adaptive entropy regulation, (4) entropy-guided particle swarm optimization, (5) optimal threshold selection and (6) final image segmentation, as shown in Figure 1. The details of each stage are presented in the following subsections.

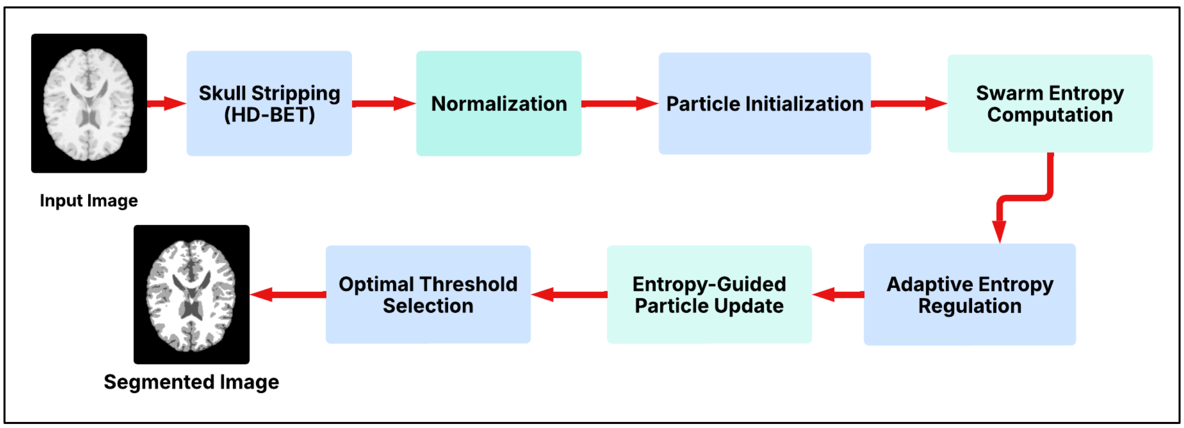

Figure 1: Block diagram of the proposed AER-PSO algorithm.

To improve numerical stability during the optimization process, the input image intensities are normalized to the range [0,1]. Image normalization minimizes the influence of intensity variations and confirms a consistent search space for particle optimization. The normalized image is computed as

$$I_{norm}(x) = \frac{I(x) - I_{min}}{I_{max} - I_{min}} \quad (1)$$

where I(x) denotes the intensity value of pixel x, and I_{min} and I_{max} represent the minimum and maximum intensity values in the input image, respectively. The normalized image I_{norm} is subsequently used as the input for the proposed AER-PSO based multilevel threshold segmentation.

Particle Initialization

Initially, a swarm consisting of N particles is randomly initialized within the predefined threshold search space. Each particle represents a candidate multilevel threshold set, where the particle position encodes the threshold values used to partition the image histogram. The position and velocity of each particle are randomly initialized within the predefined lower and upper threshold bounds of the search space.

For each particle i, the position and velocity are given by:

$$X_i = [x_{i1}, x_{i2}, ...,x_{id}] \quad (2)$$

$$V_i = [v_{i1}, v_{i2}, ...,v_{id}] \quad (3)$$

where:

- X_i represents the position vector of the i^{th} particle, corresponding to a candidate multilevel threshold set,
- V_i denotes the velocity vector of the i^{th} particle; and
- d represents the dimensionality of the search space, which is equal to the number of thresholds.

The fitness of every particle is calculated using Kapur's entropy. A higher entropy value indicates a better threshold solution. The initial personal best position of each particle is set equal to its initial position and is expressed as

$$P_{best_i} = X_i \quad (4)$$

After evaluating all particles, the particle with the highest fitness value is selected as the initial global best solution:

$$G_{best} = argmax(F_i) \quad (5)$$

where F_i denotes the fitness value of the i^{th} particle.

Swarm Entropy Computation

At each iteration, the fitness values of all particles are normalized to construct a probability distribution, which is used to estimate the diversity of the swarm. The probability associated with each particle is computed from its normalized fitness value as:

$$p_i = \frac{f_i}{\sum_{j=1}^{N} f_j} \quad (6)$$

where f_i denotes the fitness value of the i^{th} particle and $\sum_{j=1}^{N} f_j$ represents the total fitness of all particles.

The resulting particle probability distribution is expressed as

$$P = [p_1, p_2, ...p_N] \quad (7)$$

where p_i represents the normalized probability associated with the i^{th} particle.

The swarm entropy is computed using Shannon entropy:

$$H = - \sum_{i=1}^{N} p_i \, log(p_i) \quad (8)$$

where:

- H denotes swarm entropy,
- N represents the total number of particles, and
- p_i is the normalized probability of the i^{th} particle.

To preserve consistency during optimization, the computed entropy is normalized with respect to the maximum possible entropy of the swarm. A higher normalized entropy represents better swarm diversity and stronger exploration capability, on the other hand a lower entropy represents reduced diversity, suggesting that the swarm is converging toward a common region of the search space. The normalized swarm entropy is subsequently used by the adaptive entropy regulation mechanism to dynamically control the balance between exploration and exploitation during the optimization process.

Adaptive Entropy Regulation

The proposed AER-PSO algorithm dynamically regulates swarm behavior based on the normalized swarm entropy to maintain an effective balance between exploration and exploitation throughout the optimization process. When the swarm entropy falls under the lower threshold H_{low}, the swarm exhibits reduced diversity, making premature convergence to a local optimum more likely. In this situation, the inertia weight is increased to promote exploration of a wider search region. In addition, Gaussian velocity perturbation is applied to the particle velocities to diversify particle movement and enable the swarm to escape local optima.

Conversely, when the swarm entropy exceeds the upper threshold H_{high}, the swarm exhibits sufficient diversity for global exploration. Under this condition, the inertia weight is reduced to strengthen local exploitation and accelerate convergence toward promising threshold solutions. For intermediate entropy values, the adaptive mechanism keeps the current search behavior, providing a balanced transition between exploration and exploitation.

The adaptive inertia weight is computed as

$$w(t) = w_{min} + (w_{max} - w_{min})\, H(t) \quad (9)$$

where:

- w(t) denotes the adaptive inertia weight at iteration t;
- w_{min} and w_{max} represent the minimum and maximum inertia weight limits, respectively;
- H(t) denotes the normalized swarm entropy at iteration t.

After computing the adaptive inertia weight, the normalized swarm entropy is compared with the predefined thresholds H_{low} and H_{high} to regulate the particle search behavior. Depending on the swarm diversity, the algorithm either promotes exploration, strengthens exploitation, or maintains a balanced search strategy. As a result, swarm diversity is maintained, the risk of premature convergence is reduced, and the optimization process becomes more stable.

Entropy-Guided Particle Update

After adaptive entropy regulation, the particle velocities and positions are updated iteratively to search for the optimal multilevel threshold set. When the normalized swarm entropy falls below the lower threshold H_{low}, Gaussian velocity perturbation is first added to the current particle velocity to increase swarm diversity and enhance global exploration. This perturbation enables particles to escape local optima and reduces the likelihood of premature convergence. The perturbed particle velocity is computed as

$$v_i^t \leftarrow v_i^t + \alpha G \tag{10}$$

where α is the Gaussian perturbation coefficient and G~N(0,1) is a Gaussian random vector. The perturbed velocity is then used in the standard PSO velocity update. When the normalized swarm entropy is greater than or equal to H_{low}, the Gaussian perturbation step is omitted. The particle velocity is updated according to

$$v_i^{t+1} = wv_i^t + c_1r_1(P_{besti} - x_i^t) + c_2r_2\,(G_{best} - x_i^t) \tag{11}$$

where:

- w denotes the adaptive inertia weight;
- c_1 and c_2 represent the cognitive and social acceleration coefficients, respectively;
- r_1 and r_2 are uniformly distributed random numbers within the interval [0,1];
- P_{besti} denotes the personal best position of the i^{th} particle; and
- G_{best} represents the global best solution.

Using the updated velocity, the particle position is calculated as:

$$x_i^{t+1} = x_i^t + v_i^{t+1} \tag{12}$$

The updated particle positions are first evaluated against the specified search limits. Any threshold value outside the allowable range is adjusted before the fitness evaluation. Kapur's entropy is then calculated for each particle. When a particle achieves a fitness value higher than its previous best, its personal best position and the corresponding fitness value are updated. At the end of each iteration, the particle with the highest personal best fitness is taken as the global best solution. The same procedure is followed in the subsequent iterations until the convergence criterion is met or the maximum number of iterations is reached.

$$\left|G_{best}^{t+1} - G_{best}^{t}\right| < \varepsilon \tag{13}$$

where ε denotes the convergence threshold.

OPTIMAL THRESHOLD SELECTION

After the iterative optimization process terminates, the final global best particle is selected according to the highest Kapur entropy fitness value obtained during the optimization. The position of this particle represents the optimal multilevel threshold set and is expressed as

$$G_{best} = [T_1, T_2, \dots, T_k] \tag{14}$$

where k denotes the number of optimal thresholds, and the optimal threshold set is selected as

$$G_{best} = arg\,\max_{T} F_{Kapur}\,(T) \tag{15}$$

where $F_{Kapur}(T)$ represents the Kapur entropy-based fitness function. The resulting Gbest is used for the final multilevel segmentation.

FINAL SEGMENTATION

The optimal threshold set $G_{best} = [T_1, T_2, \dots, T_k]$ obtained from the AER-PSO optimization is used to partition the input image into k+1 non-overlapping intensity regions. Let I(x) denote the intensity value of pixel x, with $T_0 = I_{min}$ and $T_{k+1} = I_{max}$. The segmented image S(x) is defined as

$$S(x) = \begin{cases} C_0, T_0 \le I(x) < T_1, \\ C_i, T_i \le I(x) < T_{i+1}\,, i = 1,2,\dots,k-1, \\ C_k, T_k \le I(x) < T_{k+1} \end{cases} \tag{16}$$

C_i denotes the segmented class corresponding to the i^{th} intensity interval.

T_i represents the i^{th} optimal threshold obtained by the proposed AER-PSO algorithm.

Thus, each pixel is assigned to a class according to its intensity and the selected thresholds. The resulting S(x) is the final multilevel segmented image obtained using the proposed AER-PSO algorithm.

Algorithm 2: Adaptive Entropy-Regulated PSO (AER-PSO)

Input:

Normalised medical image I

Number of particles N

Maximum iterations T_{max}

Inertia weight limits w_{max}, w_{min}

Cognitive coefficient c_1

Social coefficient c_2

Entropy thresholds H_{low}, H_{high}

Output:

Segmented image S

Optimal threshold set $G_{best} = [T_1, T_2, \ldots, T_k]$

1. Particle Initialization

For each particle i = 1 to N

Initialize particle position X_i using Eq. (2)

Initialize particle velocity V_i using Eq. (3)

Evaluate fitness F_i using Kapur's entropy

Set personal best using Eq. (4)

End For

2. Determine Global Best

Select the particle with the highest fitness as the initial global best G_{best} using Eq. (5)

3. Main Optimization Loop

For t = 1 to T_{max}

3.1 Swarm Entropy Computation

Compute the normalized particle probability distribution using Eqs. (6) and (7)

Compute the normalized swarm entropy H(t) using Eq. (8)

3.2 Adaptive Entropy Regulation

Compute the adaptive inertia weight w(t) using Eq. (9)

If $H(t) < H_{low}$ then

Increase exploration by increasing the inertia weight

Apply Gaussian velocity perturbation to enhance exploration using Eq. (10)

Else if $H(t) > H_{high}$ then

Reduce the inertia weight to strengthen exploitation

Else

Maintain balanced exploration and exploitation

End If

3.3 Particle Update

For each particle i

Update particle velocity using Eq. (11)

Update particle position using Eq. (12)

Apply boundary constraints

Evaluate fitness using Kapur's entropy

3.4 Personal Best Update

If the current fitness is better than the personal best fitness

Update P_{besti}

End If

End For

3.5 Global Best Update

Select the particle with the highest personal best fitness

Update G_{best}

3.6 Convergence Check

Check convergence criterion using Eq. (13)

If the convergence criterion is satisfied or the maximum number of iterations is reached, then

Break

End If

End For

4. Optimal Threshold Selection

Set the final global best solution as $G_{best} = [T_1, T_2, \ldots, T_k]$ corresponding to the particle with the highest Kapur entropy fitness using Eq. (15)

5. Final Segmentation

Partition I into k+1 regions using G_{best} and Eq. (16).

Assign pixels to their corresponding classes.

Generate segmented image S.

6. Return Segmented Image S and G_{best}

End

EXPERIMENTAL RESULTS AND DISCUSSION

The proposed AER-PSO algorithm was evaluated through three experiments to assess its performance in multilevel brain magnetic resonance image (MRI) segmentation. The first experiment compares AER-PSO with existing threshold optimization algorithms using the same high-bit-depth medical image dataset employed in the CIWP-PSO study. For algorithms evaluated in the original study, the published results are reported to facilitate a direct comparison under comparable experimental conditions. The second and third experiments were conducted using the publicly available BrainWeb and Internet Brain Segmentation Repository (IBSR) datasets. Unlike the high-bit-depth medical image dataset, both BrainWeb and IBSR provide reference segmentations for quantitative evaluation. BrainWeb contains simulated brain MR images with configurable noise levels and intensity non-uniformity, whereas IBSR consists of real brain MR images with expert-annotated ground truth. For these datasets, the comparative algorithms, including CIWP-PSO, were reimplemented according to their published descriptions and evaluated using the same objective function, parameter settings, and evaluation protocol as the proposed AER-PSO. It confirmed a fair and consistent comparison across all algorithms.

EXPERIMENTAL SETUP

All experiments were implemented in Python and executed on the Google Colab platform. The same computational environment and implementation framework were used for all algorithms to provide consistent evaluation. Unless otherwise specified, the proposed AER-PSO and all comparative optimization algorithms were evaluated using identical experimental settings. The swarm size was fixed at 50 particles, the maximum number of iterations was set to 100, and multilevel thresholding was performed using 4, 6, and 8 threshold levels. Kapur's entropy was adopted as the objective function for all threshold optimization algorithms. To ensure a fair comparison with the conventional PSO algorithm, the cognitive and social acceleration coefficients were fixed at $c_1 = c_2 = 1.5$, and the particle velocities were constrained within $V_i \varepsilon [-V_{max}, V_{max}]$, where $V_{max} = 0.1\,(Var_{max} - Var_{min})$. The algorithm-specific hyperparameter settings are given in Table 1.

For the proposed AER-PSO, the inertia weight was adaptively adjusted within the range $0.4 \leq w \leq 0.9$ according to the normalized swarm entropy. The lower and upper entropy thresholds were set to $H_{low}=0.30$ and $H_{high}=0.70$, respectively. If the swarm entropy was below the lower threshold, Gaussian perturbation ($\alpha = 0.05$) and the inertia weight adjustment factor ($\Delta w = 0.05$) were used to increase swarm diversity and avoid premature convergence.

DATASET DESCRIPTION

The proposed AER-PSO algorithm was tested on two publicly available brain MRI datasets, BrainWeb and the Internet Brain Segmentation Repository (IBSR), to evaluate its segmentation performance. Both datasets provide reference segmentations for evaluating the performance of the proposed algorithm.

Table 1. Algorithm-Specific Hyperparameter Settings

Algorithm	Hyperparameters
PSO	c1 = 1.5, c2 = 1.5, w = 0.8
QPSO	c1 = 1.2, c2 = 1.2
CIWP-PSO	c1 = 1.5, c2 = 1.5, w_{min} = 0.5, w_{max} = 0.9, rate = 0.9
AER-PSO	c1 = 1.5, c2 = 1.5, w_{min} = 0.5, w_{max} = 0.9, H_{low} = 0.30, H_{high} = 0.70, Δw = 0.05, α = 0.05

BrainWeb

The BrainWeb dataset is a simulated brain MRI database containing normal and multiple sclerosis brain models with T1, T2, and Proton Density (PD)-weighted images. It also provides configurable Gaussian noise and intensity non-uniformity (INU), making it a widely used benchmark for segmentation studies. In this work, T1-weighted MRI volumes of size 181 × 217 × 181 were used. Ten axial slices (88–97) with a slice thickness of 1 mm were selected for evaluation. The proposed algorithm was tested under INU levels of 0%, 20%, and 40% and Gaussian noise levels of 3%, 7%, and 9% (BrainWeb, 2013).

Internet Brain Segmentation Repository (IBSR)

The IBSR is a publicly available clinical brain MRI dataset containing T1-weighted images with expert manual segmentations that serve as ground truth for quantitative evaluation. Each MRI volume has dimensions of 256 × 256 × 128, with voxel resolutions ranging from 0.84 × 0.84 × 1.5 mm³ to 1.0 × 1.0 × 1.5 mm³. In this study, the ANA1 images was used for evaluation. Ten axial slices (63–72) were selected, as corresponding expert-segmented reference images were available (Internet Brain Segmentation Repository, 1997).

PERFORMANCE EVALUATION METRICS

The proposed AER-PSO algorithm was evaluated using two categories of performance measures. The first includes optimization and image quality metrics: Kapur's Entropy, Peak Signal-to-Noise Ratio, Structural Similarity Index Measure, and Feature Similarity Index Measure. The second consists of ground-truth-based segmentation metrics: Segmentation Accuracy, Dice Similarity Coefficient, Jaccard Similarity Index, and Sensitivity, which measure the agreement between the segmented image and the reference annotation.

Kapur's Entropy

Kapur's Entropy was used as the objective function for multilevel threshold optimization. The threshold levels were selected by maximizing the entropy of the image histogram. A higher entropy value indicates better separation of the image regions. Using Kapur's Entropy also makes it possible to compare the proposed algorithm with other threshold-based optimization methods (Kapur et al., 1985).

Peak Signal-to-Noise Ratio (PSNR)

PSNR is used to assess the quality of the segmented image by comparing it with the original image through the Mean Squared Error (MSE). Higher PSNR values indicate better image quality (Gonzalez & Woods, 2002).

$$PSNR = 10log_{10}\left(\frac{MAX^2}{MSE}\right) \quad (17)$$

where MAX represents the maximum possible pixel intensity and MSE denotes the Mean Squared Error.

Structural Similarity Index Measure (SSIM)

SSIM was evaluated to compare the original and segmented images. A value close to 1 represents that the two images are more alike (Wang et al., 2004).

$$SSIM(A,B) = \frac{(2\mu_A\mu_B+C_1)(2\sigma_{AB}+C_2)}{(\mu_A{}^2+\mu_B{}^2+C_1)(\sigma_A{}^2+\sigma_B{}^2+C_2)} \quad (18)$$

where, μ_A and μ_B are the mean intensities of original and segmented images, $\sigma_A{}^2$ and $\sigma_B{}^2$ are the variances of original and segmented images, σ_{AB} is the covariance between original and segmented images, C_1 and C_2 are small constants to stabilize the division.

Feature Similarity Index Measure (FSIM)

FSIM computes the similarity between images based on phase congruency and gradient magnitude. Large FSIM values represent better structural preservation (Zhang et al., 2011).

$$FSIM = \frac{\sum_{x\in\Omega} S_{PC}(x)\cdot W_{PC}(x)}{\sum_{x\in\Omega} W_{PC}(x)} \quad (19)$$

$S_{PC}(x)$: Similarity measure of phase Congruency between the original and segmented images at pixel x,

$W_{PC}(x)$: Weight assigned to the phase congruency value at pixel,

Ω: Total number of pixels in the image

Segmentation Accuracy (SA)

SA is the ratio of correct pixel classification to the total number of pixels. A greater value indicates higher segmentation accuracy (Gonzalez & Woods, 2002).

$$SA = \sum_{k=1}^{C} \frac{|A_k \cap B_k|}{|A_k \cup B_k|} \quad (20)$$

A_k: Ground truth region of class, B_k: Segmented region of class, $|A_k \cap B_k|$: Correctly segmented region, $|A_k \cup B_k|$: Total region, C: Total number of segmented classes

Dice Similarity (DS)

DS measures the degree of overlap between the segmented region and the corresponding ground-truth region. Let TP, FP, and FN denote the numbers of true-positive, false-positive, and false-negative pixels, respectively. DS is defined as (Taha & Hanbury, 2015):

$$DS = \frac{2TP}{2TP + FP + FN} \quad (21)$$

Equivalently, if A and B denote the segmented and ground-truth regions, respectively, DS can be expressed in set notation as (Jafargholkhanloo et al., 2025):

$$DS\,(A,B) = \frac{2\,|A \cap B|}{|A| + |B|} \quad (22)$$

where A∩B represents the pixels correctly identified as belonging to the corresponding region.

Jaccard Similarity (JS)

JS measures the overlap between the segmented region and the ground-truth region. It is defined in terms of the confusion-matrix elements as (Taha & Hanbury, 2015):

$$JS = \frac{TP}{TP + FP + FN} \tag{23}$$

The equivalent set-based representation, based on Jafargholkhanloo et al. (2025), is given by

$$J(A,B) = \frac{|A \cap B|}{|A \cup B|} \tag{24}$$

where A∪B represents all pixels belonging to either the segmented region or the corresponding ground-truth region.

Sensitivity

Sensitivity measures the proportion of positive pixels correctly identified with respect to the ground truth. Higher Sensitivity values indicate fewer missed target pixels (Fawcett, 2005).

$$Sensitivity = \frac{TP}{TP + FN} \tag{25}$$

where TP represents correctly segmented pixels, and FN represents ground-truth pixels not identified by the segmentation method.

PERFORMANCE EVALUATION

The first experiment validates the proposed AER-PSO algorithm on the same high bit depth medical images as the original CIWP-PSO experiment. Figure 2 shows the brain tumor images and their corresponding gray-level histograms used for evaluation.

The same experimental conditions and evaluation criteria have been maintained for a fair comparison of the algorithms. The results of PSO, QPSO, and CIWP-PSO algorithms have been adopted from the original research paper, while those of the AER-PSO algorithm have been generated under similar conditions. All the algorithms have employed Kapur's Entropy as the objective function and have been evaluated at threshold levels of 4, 6, and 8. Since the optimization process is stochastic, each algorithm was executed ten times for every test image. The results are presented in Table 2.

Table 2 presents the Kapur entropy values of PSO, QPSO, CIWP-PSO, and the proposed AER-PSO for nine high-bit-depth medical images. For all four algorithms, the entropy values increase as the number of threshold levels increases. This indicates that more thresholds preserve additional image information.

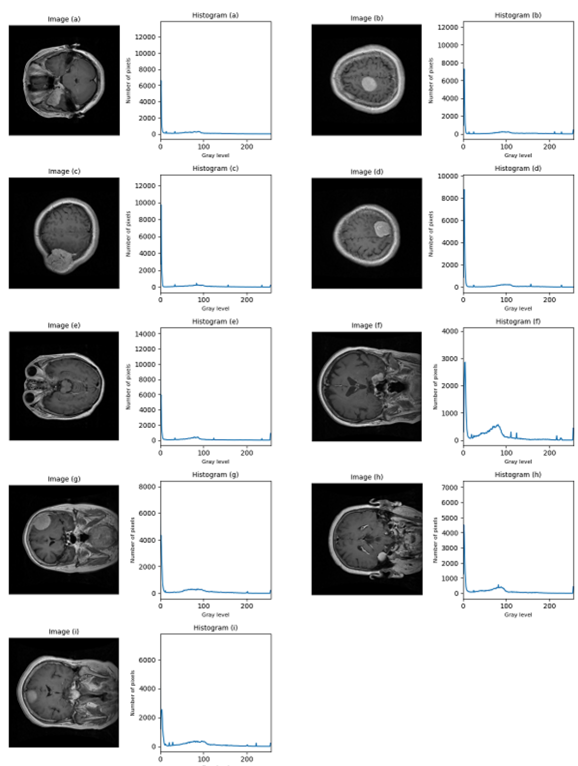

Figure 2: Brain tumor images and corresponding intensity histograms used in the experiments.

Among the four algorithms, AER-PSO gives the highest entropy values for all test cases. It gives the highest Kapur entropy value in all 27 cases, covering nine images and three threshold levels. PSO, QPSO, and CIWP-PSO give lower values in every case. The results show that AER-PSO can find better threshold values for different images and threshold levels.

The advantage of the AER-PSO approach is obvious when considering higher thresholds. For instance, when the threshold level is 8 in Image a, the AER-PSO approach provides the Kapur entropy as 49.8954, which is greater than the values of PSO, QPSO, and CIWP. Similar trends are observed for several other images.

The segmented image quality was further evaluated using PSNR, SSIM, and FSIM metrics. Unlike Kapur's Entropy that computes the optimization of the threshold, these metrics measure image fidelity, structural similarity, and features preservation. PSO, QPSO, CIWP-PSO, and AER-PSO results are presented in Tables 3–5.

Table 3 presents the PSNR values of the compared algorithms. Higher PSNR values represent lower distortion and better preservation of image information. AER-PSO produces the maximum PSNR value in 23 out of 27 instances. CIWP-PSO and QPSO produce optimal results in the rest of the 4 instances. PSO fails to provide

Table 2: Kapur entropy values obtained by various optimization algorithms.

Image	Threshold	PSO	QPSO	CIWP-PSO	AER-PSO
Image a	4	28.9278	28.8372	28.9558	29.2440
	6	39.5246	39.6761	39.5794	39.9167
	8	49.6855	49.6023	49.7089	49.8954
Image b	4	28.7852	28.7413	28.7852	28.8756
	6	39.1449	39.1564	39.1343	39.3788
	8	48.8609	49.1102	49.1231	49.6708
Image c	4	29.1776	29.1778	29.1778	29.5739
	6	39.9822	39.9458	39.9917	40.8359
	8	49.9807	50.0601	50.0902	50.4534
Image d	4	27.4075	27.4081	27.4067	27.9033
	6	37.2134	37.2098	37.2159	38.2538
	8	46.1324	46.3018	46.4223	46.9467
Image e	4	29.2959	29.2957	29.2967	29.5074
	6	40.0398	40.0612	40.0045	40.1639
	8	50.1839	49.8672	50.1997	50.9324
Image f	4	29.3867	29.3498	29.3871	29.4312
	6	39.3356	39.3481	39.3392	39.5995
	8	48.6675	48.6379	49.0636	49.3276
Image g	4	29.4967	29.4973	29.4973	30.1422
	6	40.1848	40.1816	40.1851	40.3908
	8	49.8371	50.0849	50.1022	50.9546
Image h	4	30.1068	30.1082	30.1076	30.2641
	6	40.7449	40.7319	40.7511	40.9804
	8	50.8421	50.8956	50.9613	51.1802
Image i	4	28.9570	28.9631	28.9641	29.0696
	6	39.1470	39.1514	39.1485	39.6701
	8	48.8982	48.8952	48.9058	49.1211

an optimal PSNR in any of the instances. This implies the low distortion that AER-PSO causes. Table 4 presents the SSIM values of the segmented images. Higher SSIM values indicate better preservation of image structure. AER-PSO gives the highest SSIM values at all threshold levels compared with PSO, QPSO, and CIWP-PSO. This shows that AER-PSO preserves the image structure better during multilevel threshold segmentation.

Table 5 shows the FSIM values of the segmented images. Higher FSIM values indicate better preservation of important image features. AER-

PSO gives the highest FSIM values at all threshold levels compared with PSO, QPSO, and CIWP-PSO. This shows that AER-PSO preserves important image features better during multilevel threshold segmentation.

The improved image quality of AER-PSO is attributed to its entropy-guided adaptive search strategy, which balances exploration and exploitation by adjusting the inertia weight based on swarm diversity. Swarm diversity is thus preserved, while a better threshold selection is obtained by minimizing distortion and preserving the structures and features of the images. The experimental results based on Kapur entropy, PSNR, SSIM, and FSIM metrics demonstrate that AER-PSO outperforms PSO, QPSO, and CIWP-PSO in multilevel medical image segmentation process.

Table 3: PSNR values obtained by various optimization algorithms.

Image	Threshold	PSO	QPSO	CIWP-PSO	AER-PSO
Image a	4	24.4424	24.8832	24.8856	25.7834
	6	28.0490	26.2756	28.4368	28.2345
	8	29.3914	29.9011	29.3003	30.1812
Image b	4	25.2679	25.2565	25.2679	26.6957
	6	27.0630	27.4936	27.5584	28.4641
	8	30.3192	29.8971	30.5169	31.6090
Image c	4	24.2259	24.6018	24.2281	24.3663
	6	27.9431	28.0154	27.8860	28.7396
	8	28.8074	28.8971	30.2540	31.4514
Image d	4	29.0857	29.5618	29.1042	29.9038
	6	32.0062	32.0213	32.0717	32.0789
	8	32.6642	32.4456	34.3149	34.9117
Image e	4	24.4971	24.0198	24.3406	25.9294
	6	25.6286	27.8756	27.7922	28.6328
	8	28.8294	28.2873	28.7917	29.7395
Image f	4	24.0274	23.9028	24.1172	25.6917
	6	26.2045	26.2368	26.2460	27.8180
	8	28.7626	25.9082	29.2011	30.9747
Image g	4	23.0312	24.2066	23.0009	24.1857
	6	26.9839	26.7805	26.9817	27.5068
	8	28.2808	28.2901	28.7103	29.9325
Image h	4	22.6310	20.9833	22.7016	23.8735
	6	26.5491	25.1744	26.4835	27.1205
	8	26.4006	27.3181	27.4012	28.7244
Image i	4	21.6911	21.0206	21.4545	21.8220
	6	27.2714	27.4192	27.3524	27.7876
	8	29.4433	29.3211	29.6972	29.5688

Table 4: SSIM values obtained by various optimization algorithms.

Image	Threshold	PSO	QPSO	CIWP-PSO	AER-PSO
Image a	4	0.667250	0.693592	0.711307	0.712481
	6	0.751242	0.735561	0.755320	0.778028
	8	0.762948	0.770233	0.763491	0.773491
Image b	4	0.650561	0.640713	0.652481	0.698234
	6	0.663727	0.679216	0.664423	0.671508
	8	0.696654	0.687862	0.701726	0.732223
Image c	4	0.644390	0.643562	0.644272	0.645717
	6	0.683289	0.685791	0.686394	0.698847
	8	0.689734	0.699232	0.703986	0.714060
Image d	4	0.692611	0.691846	0.693162	0.715285

	6	0.716193	0.715883	0.715679	0.724422
	8	0.722963	0.723154	0.725679	0.730367
Image e	4	0.710189	0.710931	0.710762	0.724370
	6	0.721450	0.737548	0.743791	0.767004
	8	0.750253	0.733484	0.752410	0.798997
Image f	4	0.542575	0.480349	0.546936	0.565813
	6	0.644896	0.643473	0.644780	0.644896
	8	0.671775	0.672342	0.693120	0.712636
Image g	4	0.639844	0.642374	0.639888	0.656937
	6	0.694489	0.692234	0.694551	0.727208
	8	0.713883	0.718324	0.718261	0.724769
Image h	4	0.574259	0.568923	0.579174	0.595232
	6	0.674987	0.647632	0.677113	0.685277
	8	0.688304	0.689234	0.681930	0.697228
Image i	4	0.550148	0.592342	0.542314	0.614639
	6	0.714793	0.713432	0.715605	0.727653
	8	0.740898	0.743243	0.744294	0.756211

Experimental Results on the BrainWeb Dataset

The proposed AER-PSO algorithm was evaluated on the BrainWeb simulated MRI dataset under four noise and RF bias field conditions: 3% noise with 0% RF, 3% noise with 20% RF, 7% noise with 20% RF, and 9% noise with 40% RF. Ten axial slices (88–97) were chosen for each condition, and the mean values of SA, JS, DS, Sensitivity, Kapur Entropy, PSNR, SSIM, and FSIM were calculated. Mean metric values from multiple slices were used for evaluation under different degradation conditions.

Figure 3 presents representative segmentation results of AER-PSO under four BrainWeb conditions: 3% noise with 0% RF, 3% noise with 20% RF, 7% noise with 20% RF, and 9% noise with 40% RF for slice 90. The results include the original, normalized, segmented images (Threshold levels 4,6, and 8) and ground truth. AER-PSO separates WM, GM, and CSF regions while maintaining the anatomical details of the brain. The segmentation quality is affected by increased noise and RF bias due to reduced tissue contrast; however, the obtained results remain in agreement with the ground truth. With increased threshold level, the segmented regions become more clear and the tissue boundaries are better defined.

Table 5: FSIM values obtained by various optimization algorithms.

Image	Threshold	PSO	QPSO	CIWP-PSO	AER-PSO
Image a	4	0.498133	0.502131	0.519682	0.538143
	6	0.574165	0.571233	0.587774	0.595600
	8	0.624349	0.615234	0.604338	0.638684
Image b	4	0.445692	0.445692	0.445692	0.457125
	6	0.509182	0.512343	0.503088	0.532291
	8	0.585093	0.573214	0.583868	0.603290
Image c	4	0.398926	0.409412	0.407108	0.428830
	6	0.489188	0.458765	0.490643	0.503560
	8	0.528547	0.534532	0.543275	0.559923
Image d	4	0.414142	0.434254	0.413704	0.447938
	6	0.492112	0.484352	0.488047	0.524725
	8	0.521157	0.534525	0.548054	0.551115
Image e	4	0.473258	0.523414	0.505943	0.552034
	6	0.527902	0.554235	0.569329	0.578895
	8	0.582276	0.582534	0.597466	0.616677
Image f	4	0.497257	0.434524	0.492476	0.514220
	6	0.530858	0.543523	0.525067	0.552958
	8	0.613659	0.592345	0.619356	0.629748
Image g	4	0.461028	0.464525	0.448729	0.471121

	6	0.559622	0.545635	0.560060	0.580215
	8	0.587383	0.608456	0.604149	0.626343
Image h	4	0.490482	0.484535	0.496913	0.513745
	6	0.577440	0.554366	0.564578	0.593297
	8	0.573465	0.645636	0.608605	0.658354
Image i	4	0.448682	0.447867	0.431020	0.466312
	6	0.548361	0.519435	0.527984	0.562866
	8	0.614393	0.619455	0.625999	0.630476

Figure 4 presents the segmentation results of AER-PSO for four BrainWeb T1-weighted MRI slices (88, 89, 91, and 92) with 3% noise and 20% RF bias. The results include the original, normalized, segmented images (Threshold levels 4, 6, and 8), and the corresponding ground truth. The segmented images are close to the ground truth for all four slices. Compared with the threshold level of 4, the segmentation results obtained using threshold levels of 6 and 8 show more anatomical detail and better-defined tissue boundaries.

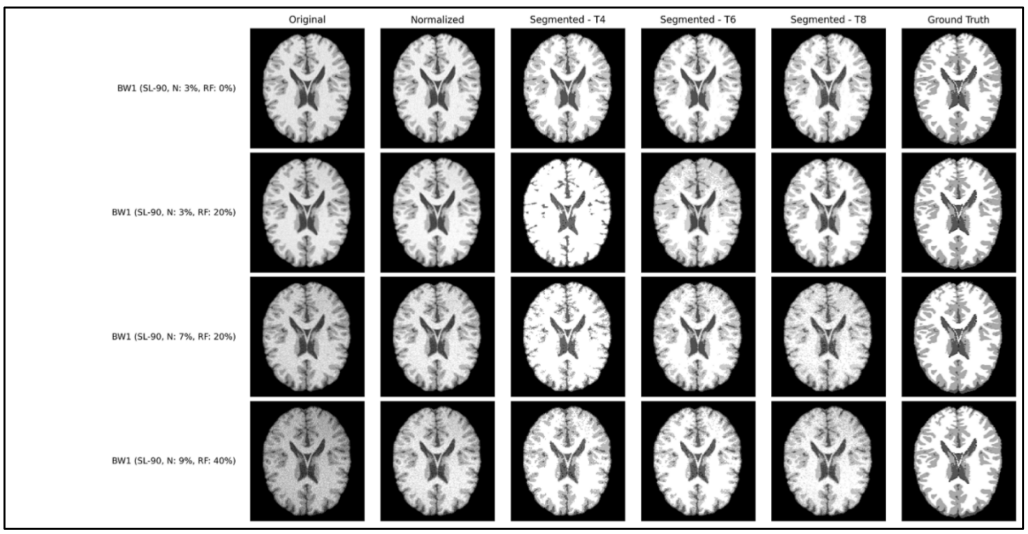

Figure 3: AER-PSO segmentation results on BrainWeb at different noise and bias-field levels.

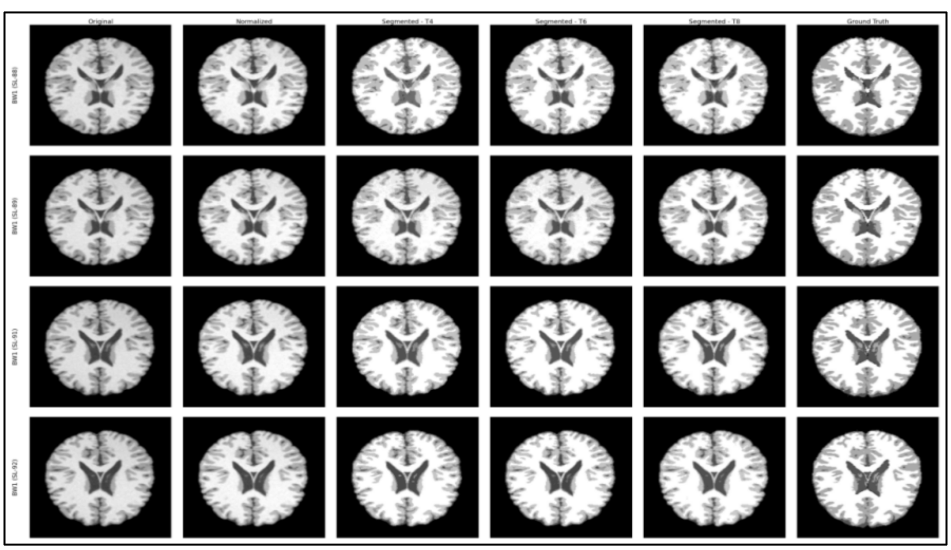

Figure 4: AER-PSO segmentation results on four BrainWeb slices with 3% noise and 20% bias field.

The same trend is observed in every slice, indicating consistent performance of the proposed AER-PSO. Table 6 summarizes the average segmentation performance of AER-PSO under four experimental conditions. As the noise level and RF bias field increase, the segmentation performance gradually decreases because tissue boundaries become less distinguishable. Nevertheless, the proposed algorithm maintains stable performance under all conditions. Under the least challenging condition (3% noise and 0% RF), increasing the threshold level from 4 to 8 improves almost every evaluation metric. Segmentation Accuracy increases from 0.8017 to 0.8538, Dice Similarity from 0.8375 to 0.8438, Jaccard Similarity from 0.7204 to 0.7298, and Sensitivity from 0.8412 to 0.8575. Kapur Entropy increases from 24.8960 to 45.8823, while PSNR increases from 29.1224 to 34.2819, representing better preservation of the segmented image.

Table 6: Mean AER-PSO performance on BrainWeb under different noise and bias-field conditions (Slices 88–97).

Noise+RF(%)	Threshold	SA	JS	DS	Sen	Kapur	PSNR	SSIM	FSIM
3% N + 0% RF	4	0.8017	0.7204	0.8375	0.8412	24.8960	29.1224	0.739990	0.716189
	6	0.8108	0.7115	0.8314	0.8446	39.7175	31.9171	0.740669	0.702942
	8	0.8538	0.7298	0.8438	0.8575	45.8823	34.2819	0.759444	0.691584
3%N+ 20% RF	4	0.7886	0.6779	0.8080	0.7995	24.3503	27.8156	0.713697	0.690689
	6	0.8068	0.6982	0.8220	0.8172	39.1169	30.2957	0.721573	0.704199
	8	0.8516	0.7163	0.8347	0.8618	43.5387	32.6577	0.743639	0.718791
7%N+ 20% RF	4	0.8038	0.6753	0.8062	0.8046	23.8637	27.3318	0.704151	0.684953
	6	0.8004	0.6584	0.7940	0.7879	38.8200	28.7891	0.712894	0.675426
	8	0.7989	0.6464	0.7852	0.7868	42.7668	29.6926	0.721609	0.661620
9%N+ 40% RF	4	0.7886	0.6090	0.7570	0.7584	22.8923	26.6028	0.698208	0.683217
	6	0.7786	0.5739	0.7293	0.7249	37.9273	27.9374	0.709960	0.679219
	8	0.7769	0.5734	0.7289	0.7279	41.1778	30.4458	0.714304	0.656000

As the imaging conditions become more difficult, the segmentation performance gradually decreases. Under the most severe condition (9% noise and 40% RF), the Segmentation Accuracy at threshold level 8 decreases from 0.8538 to 0.7769. Similarly, Dice Similarity decreases from 0.8438 to 0.7289, Jaccard Similarity from 0.7298 to 0.5734, Sensitivity from 0.8575 to 0.7279, and PSNR from 34.2819 to 30.4458. Despite these reductions, AER-PSO continues to produce satisfactory segmentation results under different imaging conditions. Table 6 also shows the effect of the threshold level. The results show that increasing the number of thresholds improves Segmentation Accuracy, Dice Similarity, Sensitivity, Kapur Entropy, and PSNR. Among the evaluated threshold levels, the eight-threshold setting provides the most favorable overall performance. Table 7 compares the average segmentation performance of PSO, QPSO, CIWP-PSO, and AER-PSO under 3% noise and 20% RF bias for threshold levels 4, 6, and 8. For threshold level 4, AER-PSO gives the highest Segmentation Accuracy (0.7886) and Sensitivity (0.7995). CIWP-

PSO gives slightly higher Jaccard Similarity and Dice Similarity, but the differences from AER-PSO are very small. For threshold level 6, AER-PSO records the highest values for all four segmentation metrics. The same trend can be seen at threshold level 8. AER-PSO gives the highest Segmentation Accuracy (0.8516), Jaccard Similarity (0.7163), Dice Similarity (0.8347), and Sensitivity (0.8618). Compared with various algorithms, AER-PSO gives higher values for all four segmentation metrics. The difference becomes clearer at higher threshold levels.

Table 7: Mean segmentation performance of all algorithms on BrainWeb at 3% noise and 20% RF (Slices 88–97).

Threshold	Metric	PSO	QPSO	CIWP-PSO	AER-PSO
4	SA	0.7418	0.7639	0.7625	0.7886
	JS	0.6175	0.6274	0.6794	0.6779
	DS	0.7637	0.7710	0.8091	0.8080
	Sensitivity	0.7522	0.7748	0.7736	0.7995
6	SA	0.7794	0.7802	0.7993	0.8068
	JS	0.6399	0.6405	0.6948	0.6982
	DS	0.7804	0.7809	0.8199	0.8220
	Sensitivity	0.7899	0.7908	0.8099	0.8172
8	SA	0.8034	0.8291	0.8395	0.8516
	JS	0.6582	0.6606	0.6916	0.7163
	DS	0.7938	0.7956	0.8177	0.8347
	Sensitivity	0.8138	0.8397	0.8499	0.8618

Table 8. Mean image quality performance metrics of all algorithms on the BrainWeb (3% noise and 20% RF bias field, Slices 88–97).

Threshold	Metric	PSO	QPSO	CIWP-PSO	AER-PSO
4	Kapur	24.0249	24.1349	24.2931	24.3503
	PSNR	27.0676	27.1721	27.7006	27.8156
	SSIM	0.694188	0.699254	0.700716	0.713697
	FSIM	0.672121	0.674529	0.679352	0.690689
6	Kapur	38.3437	38.3722	38.6977	39.1169
	PSNR	29.2154	29.4527	29.5437	30.2957
	SSIM	0.718786	0.716333	0.713119	0.721573
	FSIM	0.701667	0.702488	0.704542	0.704199
8	Kapur	43.0755	43.1339	43.3628	43.5387
	PSNR	30.5159	30.9875	31.1996	32.6577
	SSIM	0.740799	0.743697	0.744662	0.743639
	FSIM	0.715178	0.716428	0.717615	0.718791

Table 8 compares PSO, QPSO, CIWP-PSO, and AER-PSO using Kapur Entropy, PSNR, SSIM, and FSIM under 3% noise and 20% RF bias. AER-PSO gives the highest Kapur Entropy values at all threshold levels.

The entropy increases from 24.3503 at threshold level 4 to 39.1169 at threshold level 6 and 43.5387 at threshold level 8, indicating improved threshold selection by AER-PSO. The PSNR value of AER-PSO is the highest at threshold levels 4 and 6. It increases from 27.8156 at threshold level4 to 30.2957 at threshold level 6 and remains higher than the values obtained by PSO, QPSO, and CIWP-PSO. At threshold level 8, AER-PSO gives a PSNR value of 32.6577, which is higher than the values obtained by CIWP-PSO, QPSO, and PSO. For SSIM, AER-PSO achieves the maximum values at threshold level 4 (0.713697) and threshold level 6 (0.721573). The SSIM value of CIWP-PSO is 0.744662 at threshold level 8 and slightly higher than that of AER-PSO, which is 0.743639. The FSIM values show a similar trend. The highest value of AER-PSO occurs at threshold level 4 (0.690689) and threshold level 8 (0.718791). However, CIWP-PSO achieves slightly higher value at threshold level 6. Taken together, it can be seen that AER-PSO does well on all four evaluation metrics.

The BrainWeb results demonstrate the effectiveness of AER-PSO for multilevel brain MRI image segmentation. Under different noise levels, RF bias field conditions, and threshold levels, AER-PSO consistently achieves higher values of Segmentation Accuracy, Jaccard Similarity, Dice Similarity, Sensitivity, Kapur Entropy, PSNR, SSIM, and FSIM than PSO, QPSO, and CIWP-PSO. These results show that AER-PSO performs well for multilevel brain MRI segmentation under different imaging conditions.

Experimental Results on Real-World Dataset

To evaluate the proposed AER-PSO on real clinical data, experiments were conducted using the IBSR dataset. The evaluation used ten T1-weighted MRI slices (63–72) with their corresponding expert-annotated ground truth. Unlike the simulated BrainWeb dataset, IBSR contains real MRI images with anatomical variations, intensity inhomogeneity, and imaging artifacts, leading to a more challenging segmentation task.

Figure 5 shows representative segmentation results of the proposed AER-PSO on two IBSR axial slices (63 and 66). For each slice, the original image, normalized image, segmented results at threshold levels 4, 6, and 8, and the corresponding expert-annotated ground truth are presented. The results show that AER-PSO separates the major brain tissues while preserving anatomical structures. The segmented images show gradual improvement as the threshold level increases from threshold level 4 to threshold level 8. Among the three threshold levels, threshold level 8 shows the closest match to the ground truth, with only small differences at the tissue boundaries.

Figure 6 compares the class-wise segmentation produced by AER-PSO with the corresponding IBSR ground truth for slices 63, 66, and 71. The columns display the Background, CSF, GM, and WM classes, while the rows show the AER-PSO segmentation and the expert annotations. Only small differences are found between the segmented tissues and the ground truth near the CSF regions and tissue boundaries. The results indicate that AER-PSO preserves the anatomical structures and gives consistent segmentation across different slices.

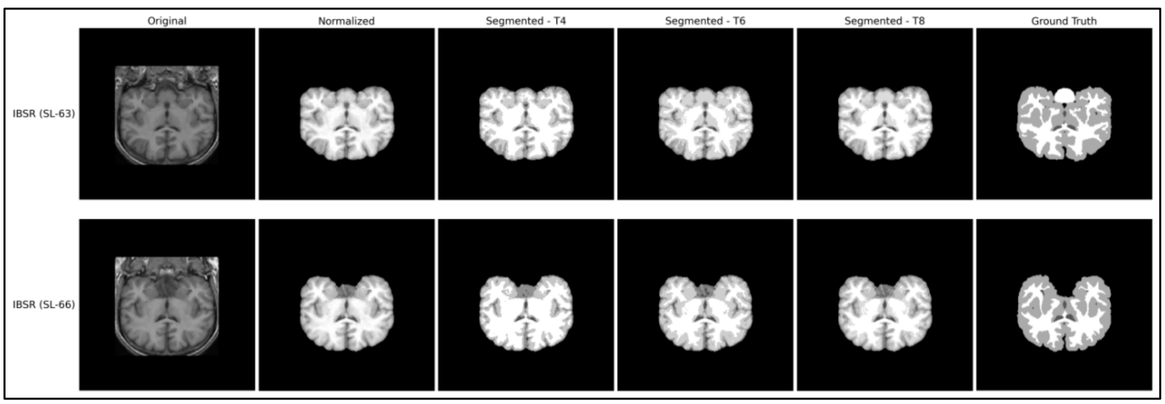

Figure 5: Segmentation results of AER-PSO on the IBSR dataset for slices 63 and 66 at threshold levels 4, 6, and 8.

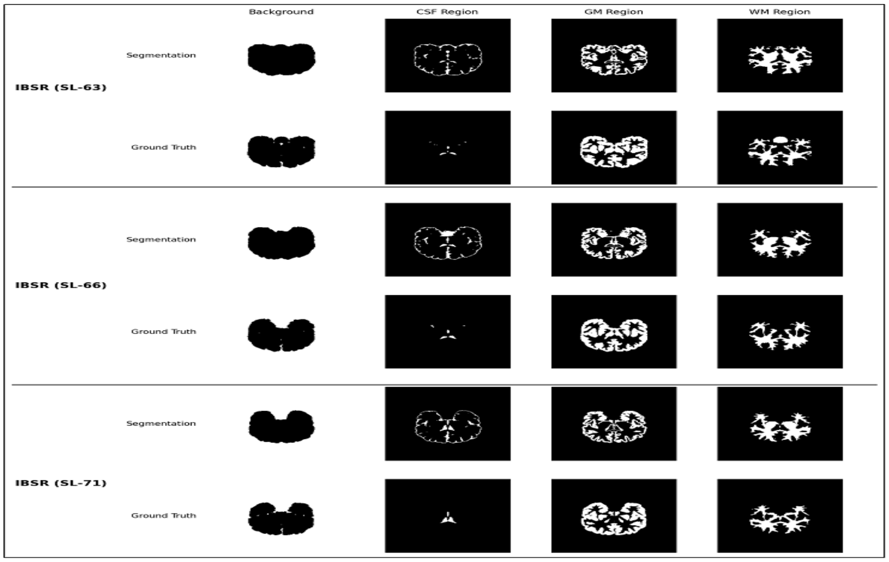

Figure 6: Class-wise AER-PSO segmentation results and ground truth on the IBSR dataset for three slices.

Table 9 compares the mean Kapur Entropy, PSNR, SSIM, and FSIM values of PSO, QPSO, CIWP-PSO, and AER-PSO on the IBSR dataset for threshold levels 4, 6, and 8. AER-PSO gives the highest Kapur Entropy and PSNR at all three threshold levels. The Kapur Entropy increases from 22.8329 at threshold level 4 to 38.4590 at threshold level 6 and 41.8194 at threshold level 8. Similarly, the PSNR increases from 26.5588 to 29.6984 and 30.3978.

AER-PSO obtains SSIM values of 0.683451, 0.693914, and 0.709741 for threshold levels 4, 6, and 8, respectively. The corresponding FSIM values are 0.675678, 0.689671, and 0.708726. Table 10 compares the segmentation performance using SA, JS, DS, and Sensitivity. The SA improves from 0.7481 at threshold level 4 to 0.7593 at threshold level 6 and 0.8094 at threshold level 8. At each threshold level, the SA obtained by AER-PSO is higher than that of PSO, QPSO, and CIWP-PSO.

The overlap-based metrics also favour AER-PSO. At threshold level 4, the highest Jaccard Similarity (0.6758) and Dice Similarity (0.8065) are obtained by AER-PSO. Similar results are obtained at threshold levels 6 and 8, where AER-PSO records the highest JS (0.6904 and 0.6864) and DS (0.8168 and 0.8140).

Table 9. Mean segmentation performance metrics of all algorithms on the IBSR dataset (slices 63–72).

Threshold	Metric	PSO	QPSO	CIWP-PSO	AER-PSO
4	Kapur	22.1458	22.7427	22.8329	22.8329
	PSNR	26.2663	26.5447	26.5359	26.5588
	SSIM	0.663323	0.663428	0.676730	0.683451
	FSIM	0.652334	0.653456	0.655123	0.675678
6	Kapur	37.5787	37.8422	37.8470	38.4590
	PSNR	27.1741	27.4883	27.6161	29.6984
	SSIM	0.684576	0.685681	0.687395	0.693914
	FSIM	0.681804	0.682421	0.683424	0.689671
8	Kapur	41.3167	41.4047	41.3188	41.8194
	PSNR	28.8098	28.9877	29.0887	30.3978
	SSIM	0.691862	0.692782	0.692887	0.709741
	FSIM	0.692887	0.693812	0.694412	0.708726

Table 10. Mean image quality performance metrics of all algorithms on the IBSR dataset (Slices 63–72).

Threshold	Metric	PSO	QPSO	CIWP-PSO	AER-PSO
4	SA	0.7294	0.7388	0.7388	0.7481
	JS	0.5915	0.6239	0.6558	0.6758
	DS	0.7433	0.7684	0.7923	0.8065
	Sensitivity	0.7450	0.7606	0.7656	0.7876
6	SA	0.7357	0.7398	0.7436	0.7593
	JS	0.6347	0.6254	0.6593	0.6904
	DS	0.7766	0.7695	0.7946	0.8168
	Sensitivity	0.7745	0.7876	0.8093	0.8159
8	SA	0.7407	0.7562	0.7881	0.8094
	JS	0.6484	0.6473	0.6610	0.6864
	DS	0.7867	0.7859	0.7958	0.8140
	Sensitivity	0.7937	0.7969	0.8065	0.8264

AER-PSO also gives the highest Sensitivity, increasing from 0.7876 at threshold level 4 to 0.8264 at threshold level 8. All algorithms obtain slightly lower values on IBSR than on BrainWeb because IBSR contains real clinical MRI images with anatomical variability and imaging artifacts.

Among the compared algorithms, AER-PSO gives the highest Jaccard Similarity and Dice Similarity on both datasets. On BrainWeb, the highest values are 0.7163 (JS) and 0.8347 (DS) at threshold level 8, while the corresponding IBSR values are 0.6864 and 0.8140. Although the values are slightly lower on IBSR, the performance remains stable. Compared with PSO, QPSO, and CIWP-PSO, AER-PSO gives higher segmentation performance, especially at higher threshold levels. The IBSR results, together with the BrainWeb evaluation, show that AER-PSO is effective for multilevel brain MRI image segmentation and performs well on both simulated and real MRI datasets.

CONCLUSION AND FUTURE SCOPE

In this paper, an AER-PSO algorithm is proposed for multilevel threshold-based image segmentation. The proposed algorithm uses normalized swarm entropy to measure swarm diversity and adjust the inertia weight during the optimization process. Gaussian velocity perturbation is applied when the swarm diversity is low to increase population diversity, improve exploration, and reduce the chance of premature convergence. Kapur's entropy is adopted as the objective function to identify optimal multilevel threshold values for image segmentation.

The effectiveness of the proposed algorithm was first evaluated on the same high-bit-depth medical image dataset employed in the original CIWP-PSO study and subsequently validated on the publicly available BrainWeb and IBSR datasets. Experimental results showed that AER-PSO consistently achieved superior optimization and segmentation performance compared with PSO, QPSO, and CIWP-PSO. The proposed algorithm achieved higher Kapur entropy values and yielded segmented images with improved PSNR, SSIM, FSIM, SA, DS, JS, and Sensitivity. The improved performance of AER-PSO is mainly due to the entropy-based adaptive search mechanism, which controls the balance between exploration and exploitation based on swarm diversity. The adjustment of inertia weight and the use of Gaussian perturbation during low-diversity conditions help maintain diversity and select suitable threshold values. In future work, AER-PSO can be extended to other image segmentation problems, such as remote sensing, hyperspectral, underwater, and industrial images. It can also be combined with other optimization algorithms to improve segmentation performance.

Source of support: None

Conflict of interest: None.

ACKNOWLEDGEMENT

We acknowledge the support of the PG & Research Department of Computer Science, Jamal Mohamed College (Autonomous), Trichy for providing computational resources. This research was not supported by any specific grant from funding agencies in the public, commercial, or not-for-profit sectors.

REFERENCES

BrainWeb.[Dataset]. https://brainweb.bic.mni.mcgill.ca/brainweb/anatomic_normal.html

Chakraborty, R., Verma, G., & Namasudra, S. (2020). IFODPSO-based multi-level image segmentation scheme aided with Masi entropy. Journal of Ambient Intelligence and Humanized Computing, 12(7), 7793–7811.

Dhieb, M., & Frikha, M. (2016). A multilevel thresholding algorithm for image segmentation based on particle swarm optimization. In 2016 IEEE/ACS 13th International Conference of Computer Systems and Applications (AICCSA) (pp. 1–7). IEEE.

Dixit, A., & Nanda, A. (2019). Brain MR image classification via PSO based segmentation. In 2019 Twelfth International Conference on Contemporary Computing (IC3) (pp. 1–5). IEEE.

Fawcett, T. (2005). An introduction to ROC analysis. Pattern Recognition Letters, 27(8), 861–874. https://doi.org/10.1016/j.patrec.2005.10.010

Gonzalez, R. C., & Woods, R. E. (2002). Digital image processing (2nd ed.). Prentice Hall.

Internet Brain Segmentation Repository. [Dataset]. https://www.nitrc.org/projects/ibsr

Jafargholkhanloo, A.F., Shamsi, M., Bawil, M.B., & Danishvar, S. (2025). A new fuzzy clustering algorithm for image segmentation. International Journal of Fuzzy Systems.

Kapur, J., Sahoo, P., & Wong, A. (1985). A new method for gray-level picture thresholding using the entropy of the histogram. Computer Vision Graphics and Image Processing, 29(3), 273–285.

Kennedy, J., & Eberhart, R. (2002). Particle swarm optimization. In Proceedings of ICNN'95—International Conference on Neural Networks (pp. 1942–1948). IEEE.

Lan, K., Zhou, J., Jiang, X., Wang, J., Huang, S., Yang, J., Song, Q., Tang, R., Gong, X., Liu, K., Wu, Y., & Li, T. (2022). Group theoretic particle swarm optimization for multi-level threshold lung cancer image segmentation. Quantitative Imaging in Medicine and Surgery, 13(3), 1312–1322.

Li, D., Deng, N., & Chen, X. (2019). Level set medical image segmentation aided by cooperative quantum particle optimization with Lévy flights. Vibroengineering PROCEDIA, 28, 93–98.

Liang, J., Qin, A., Suganthan, P., & Baskar, S. (2006). Comprehensive learning particle swarm optimizer for global optimization of multimodal functions. IEEE Transactions on Evolutionary Computation, 10(3), 281–295.

Lokhande, N. M., & Pujeri, R. V. (2018). Novel image segmentation using particle swarm optimization. In Proceedings of the 2018 8th International Conference on Biomedical Engineering and Technology (ICBET '18) (pp. 46–50). Association for Computing Machinery.

Ma, J., & Hu, J. (2024). An improved particle swarm optimization for multilevel thresholding medical image segmentation. PLoS ONE, 19(12), 1–24.

Mahalakshmi, S., & Velmurugan, T. (2015). Detection of Brain Tumor by Particle Swarm Optimization using Image Segmentation. Indian Journal of Science and Technology, 8(22).

Maitra, M., & Chatterjee, A. (2007). A hybrid cooperative–comprehensive learning based PSO algorithm for image segmentation using multilevel thresholding. Expert Systems With Applications, 34(2), 1341–1350.

Nie, F., Liu, M., & Zhang, P. (2024). Multilevel thresholding with divergence measure and improved particle swarm optimization algorithm for crack image segmentation. Scientific Reports, 14(1), 7642.

Pal, N. R., & Pal, S. K. (1993). A review on image segmentation techniques. Pattern Recognition, 26(9), 1277–1294.

Pham, D. L., Xu, C., & Prince, J. L. (2000). Current methods in medical image segmentation. Annual Review of Biomedical Engineering, 2(1), 315–337.

Sahoo, P., Soltani, S., & Wong, A. (1988). A survey of thresholding techniques. Computer Vision Graphics and Image Processing, 41(2), 233–260.

Saifullah, S., & Dreżewski, R. (2024). Advanced medical image segmentation enhancement: a Particle-Swarm-Optimization-Based histogram equalization approach. Applied Sciences, 14(2), 923.

Sekar, B., & Parthasarathy, S. (2025). Empirical analysis on retinal segmentation using PSO-based thresholding in diabetic retinopathy grading. Biomedizinische Technik/Biomedical Engineering, 70(3), 217–227.

Taha, A. A., & Hanbury, A. (2015). Metrics for evaluating 3D medical image segmentation: analysis, selection, and tool. BMC Medical Imaging, 15(1), 29.

Tan, T. Y., Zhang, L., Lim, C. P., Fielding, B., Yu, Y., & Anderson, E. (2019). Evolving ensemble models for image segmentation using enhanced particle swarm optimization. IEEE Access, 7, 34004–34019.

Wang, Z., Bovik, A., Sheikh, H., & Simoncelli, E. (2004). Image quality assessment: from error visibility to structural similarity. IEEE Transactions on Image Processing, 13(4), 600–612.

Zhang, L., Zhang, L., Mou, X., & Zhang, D. (2011). FSIM: a feature similarity index for image Quality assessment. IEEE Transactions on Image Processing, 20(8), 2378–2386.

Zheng, J., Gao, Y., Zhang, H., Lei, Y., & Zhang, J. (2022). OTSU Multi-Threshold Image Segmentation based on improved particle swarm Algorithm. Applied Sciences, 12(22), 1151.